Contents lists available at ScienceDirect

Applied Surface Science

Full Length Article

Linear arrays of InGaAs quantum dots on nanostructured GaAs-on-Si substrates

Paloma Tejedor [a,*], Elisa García-Tabarés [b], Beatriz Galiana [b], Luis Vázquez [a], Basilio J. García [c]

[a] *Instituto de Ciencia de Materiales de Madrid, C.S.I.C. Sor Juana Inés de la Cruz 3, 28049 Madrid, Spain*
[b] *Physics Department, Universidad Carlos III de Madrid, Av. de la Universidad, 30, 2891 Leganés, Madrid, Spain*
[c] *Applied Physics Department, Universidad Autónoma de Madrid (UAM), Avda. Francisco Tomás y Valiente, 7, 28049 Madrid, Spain*

ABSTRACT

Linear arrays of high-quality quantum dots (QD) integrated in Si are an ideal platform in exploring the manipulation and transmission of quantum information. Understanding QD self-organization mechanisms on substrates compatible with Si technology is therefore of great practical importance. Here we demonstrate the epitaxial growth of linear arrays of InAs and InGaAs QDs from As_2 and In molecular beams on bare and GaAs-coated Si(001) substrates, patterned by high-resolution laser interference nanolithography. Atomic force microscopy, in combination with high-resolution scanning and transmission electron microscopies, show that these arrays exhibit an improvement in growth selectivity, lateral order and size uniformity of the QDs when a pseudomorphic 1 nm-thick GaAs buffer layer is grown prior to InAs deposition. In addition, preferential nucleation of $In_xGa_{1-x}As$ QDs along the $\langle 110 \rangle$ -oriented edges of the nanostructured GaAs-on-Si(001) substrate results from In adatom migration from (111) to (001) nanofacets and the erosion of the wetting and buffer layers caused by the Ga-In intermixing at the step edge during the Stranski-Krastanov transition. These are key elements in the formation of linear arrays of coherent QDs, which differ in morphology and structure from those obtained on both GaAs(001) and Si(001) planar surfaces.

1. Introduction

Semiconductor QDs are nanoscale structures that exhibit three-dimensional confinement of individual charge carriers, leading to atomic-like discrete energy levels [1]. Due to the existence of confined energy states in QDs, their optical and electronic properties can be tuned by changing their size and composition. This has enabled the realization of a wide variety of advanced optoelectronic and quantum devices such as low-threshold, high-temperature lasers [2–4]; high-performance optical amplifiers [5]; low, dark-current photodetectors [6]; single photon emitters [7]; and spin qubits [8].

Self-organized growth of coherent (i.e., dislocation-free and, hence, strained) InAs QDs on GaAs, the most thoroughly studied QD material system [9–12], occurs on the (001)-oriented surface during molecular-beam epitaxy (MBE) [13] or metalorganic chemical vapor deposition (MOCVD) [14] via a modified Stranski-Krastanov (S-K) mechanism [15]. In this growth mode, a two-dimensional (2D) wetting layer develops prior to the formation of three-dimensional (3D) islands. This 2D-to-3D growth mode transition is triggered by upward adatom diffusion

from the wetting layer and at the island edges [16]. By contrast, InAs growth on (110)- and (111)-oriented GaAs follows a 2D layer-by-layer mode where strain relief occurs through the formation of misfit dislocations [17,18]. The formation of InAs QD on Si, on the other hand, has been reported to occur via the S-K growth mode on both (001)- and (111)-oriented substrates. In this case, unlike growth on GaAs(001), the 3D islands are fully relaxed and contain misfit dislocations [19–21]. For most device applications, individual QDs are required to have high structural (defect-free) and optical quality. In addition, their fabrication process should be able to provide large-area, long-range ordered arrays of QDs with high uniformity in size, shape and composition [22–24]. Given that self-organized growth leads to a random distribution of QDs across the surface, a great research effort has been made in the last decades to achieve site control of QD nucleation by selective epitaxy on patterned substrates, fabricated by a variety of lithography techniques [25–27] such as electron-beam lithography, nanoimprint lithography, block copolymer lithography, or AFM-assisted lithography. Besides, the high performance recently achieved in epitaxial InAs QD devices grown on Si [28–30] points to the need of replacing current heterogeneous

integration (i.e., III-V materials bonded to a SOI substrate) by direct epitaxial integration of QD devices in a complementary metal–oxidesemiconductor (CMOS)-compatible Si platform. This would help reduce mass-production manufacturing costs and complexity while increasing its scalability [31,32].

Linear arrays of semiconductor QDs offer great prospects for high-fidelity quantum information transfer in fault-tolerant quantum computers. Nowadays, different methods for quantum state transfer are being explored to achieve connectivity beyond nearest-neighbor exchange [33–36]. Of particular interest for intermediate-scale quantum state transfer (QST) protocols that are effective at 50 nm to 10 μm length scales is the approach reported by Mills et al. [37], which consisted in shuttling an electron across a linear array of 9 Si QDs in $\sim$ 50 ns via a series of pairwise inter-dot charge transfer. Electron shuttling has been applied to other semiconductor materials, e.g., GaAs, InAs, InSb [38] while the virtual gate approach used in reference [37] could be extended to larger 1D and 2D arrays of QDs. The purpose of the present work is the creation of linear arrays formed by epitaxial In$_x$Ga$_{1-x}$As QDs through a scalable and Si CMOS-compatible process to be used as a platform to study electron charge transfer at intermediate length scales in future experiments. To this end, we have investigated the MBE growth of QDs via the Stranski-Krastanov mechanism on nanostructured Si(0 0 1) substrates, where orthogonal ⟨1 1 0⟩ -oriented edges had been defined by laser interference nanolithography. In the following, we demonstrate that the preferential nucleation of linear chains of InGaAs QDs along both ⟨1 1 0⟩ directions leads to an improvement in selectivity, lateral order and size uniformity of the dots when an ultra-thin GaAs buffer layer is grown prior to InAs deposition. Furthermore, we discuss the differences in growth morphology and structure found in dots grown on ⟨1 1 0⟩ -oriented edges with respect to those nucleated on planar (0 0 1) nanofacets of the GaAs-coated Si(0 0 1) substrate in terms of the increased mass transfer to the growing 3D islands coming from adjacent (1 1 1) nanofacets and from the underlying buffer and wetting layers via step edge erosion during the Stranski-Krastanov transition.

2. Material and methods

The experiments described in this work were carried out in a solid-source RIBER Compact-12 III-V MBE system equipped with a 10 keV electron gun for reflection high-energy electron diffraction (RHEED) measurements. Arsenic was supplied using a Mark V (Veeco) valved cracker cell working at 880 °C, which provided mechanical control over the resulting As$_2$ flux. Elemental Ga and In were supplied by conventional effusion cells. The fluxes of the Ga, In and As$_2$ beams were calibrated using the RHEED intensity oscillation technique on a GaAs (0 0 1) substrate with the aid of a kSA-400 analysis system. Atomic hydrogen was generated in a thermal cracker cell by dissociation of H$_2$ gas at a W filament heated to 1,800 °C. Nanostructured Si (0 0 1) wafers were used as deposition substrates. They were fabricated by high-resolution Lloyd's mirror laser interference nanolithography and selective reactive ion etching using CHF$_3$ and SF$_6$ gases. Prior to the introduction of the Si substrates in the MBE system, they were dipped in a HF/H$_2$O (1:10) solution for 1–2 min to remove the native oxide, rinsed thoroughly in running D.I·H$_2$O and dried with N$_2$ gas. They were subsequently exposed to O$_3$ UV for 30 min and, once in the growth chamber, exposed to an atomic H beam up to a substrate temperature of 640 °C to create double steps on the surface [39]. The substrates were then cooled down to 460 °C [40] to deposit one monolayer (ML) of As on the Si surface. Subsequently, two sets of samples were grown on the substrates thus prepared. In the first of these sets, InAs samples, having different nominal thicknesses, were deposited at 0.1 ML s^{-1} on the As-terminated Si template at 490 °C with an As/In flux ratio of 32 to induce the formation of QDs. The desorption of In from the Si surface starts to be significant at growth temperatures above 450 °C [19,21], leading to a decrease of the In sticking coefficient [41,42]. For this reason, InAs had to be supplied in excess at the temperature of our experiments in order to
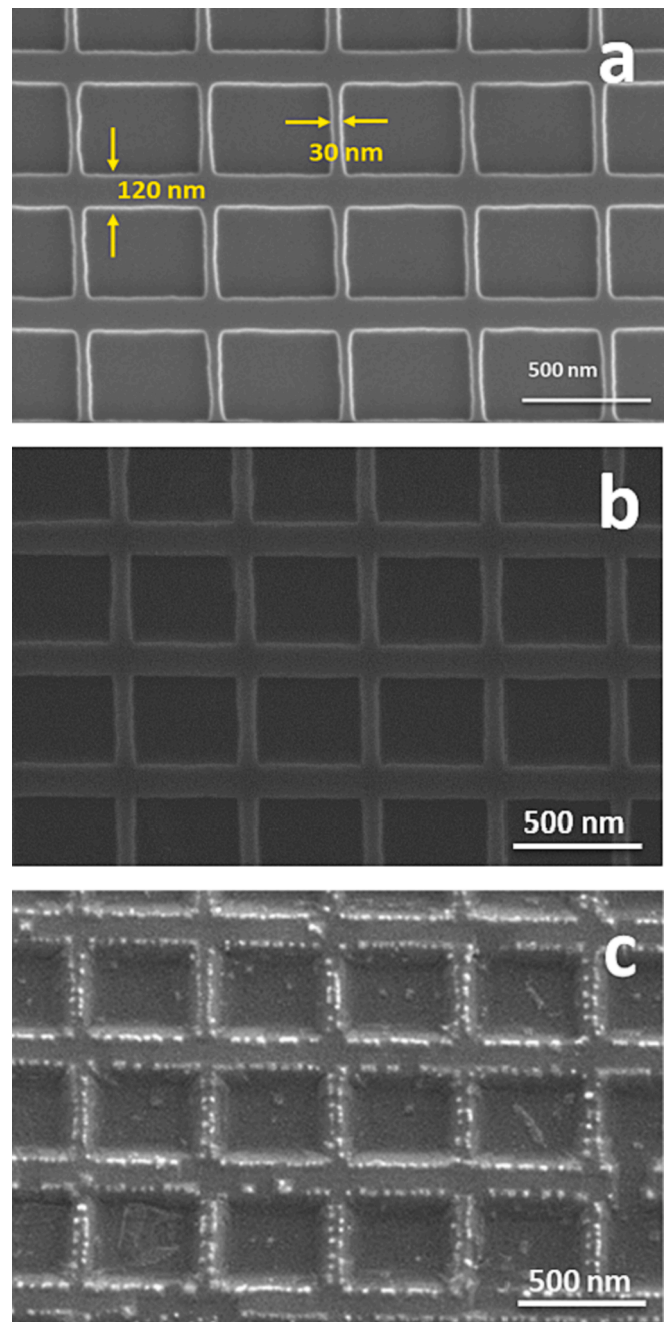

Fig. 1. High-resolution scanning electron micrographs (HRSEM) of (a) the nanostructured Si substrate and the same substrate after deposition of (b) 100 ML InAs and (c) 125 ML InAs.

achieve an effective 2 ML InAs coverage, i.e., InAs critical thickness on Si [19,21], leading to the 2D-to-3D growth mode transition on the Si surface. Since the value of the In sticking coefficient during growth of InAs on Si at 490 °C has not been previously reported, the growth mode was investigated using excess InAs supplies up to a nominal thickness of 230 ML. In the second set of samples, which were also grown at 490 °C, an ultra-thin (~1 nm) GaAs buffer layer was first deposited on the As-terminated Si surface. On this GaAs-coated Si substrate, 2 ML InAs were deposited at different growth rates and subsequently covered with a 5 nm-thick GaAs capping layer. The GaAs epilayers were grown at 0.4 ML.s^{-1} with an As/Ga flux ratio of 4 while the InAs QDs were grown at 0.1 ML s^{-1} or 0.2 ML s^{-1} with As/In flux ratios of 32 and 16, respectively. The B.E.P. of As$_2$ was kept constant at $\sim$ 4 × 10^{-7} Torr in all
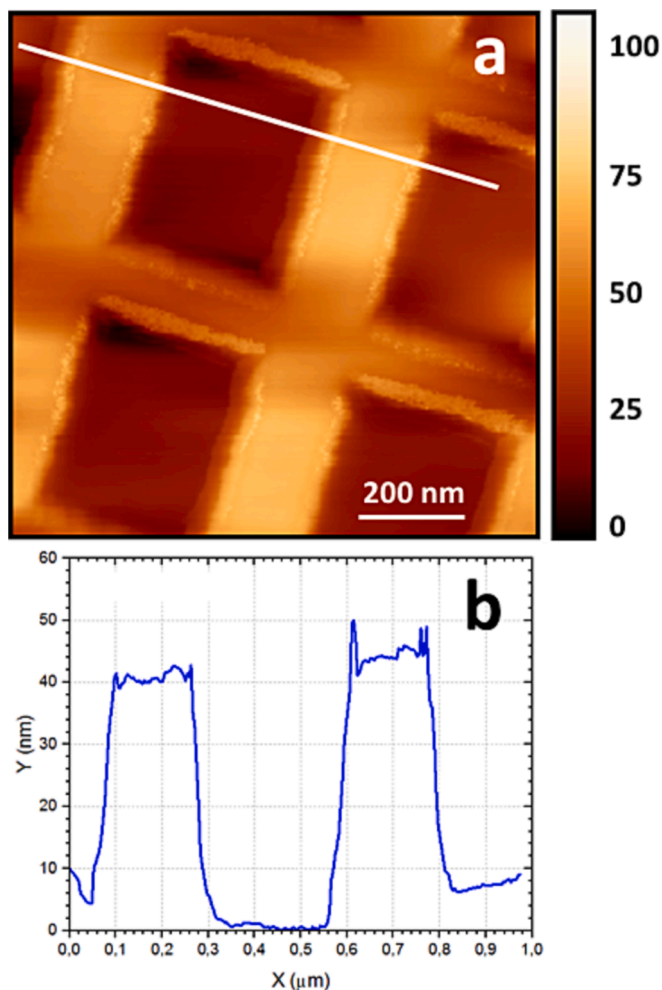
Fig. 2. (a) AFM image and (b) linear profile showing the decoration of $\langle 1\,1\,0 \rangle$ oriented edges of the Si nanotemplate after deposition of 100 ML InAs (image size: 1 μm × 1 μm).

experiments. For all samples, the substrate temperature was lowered to room temperature at a rate of 5 deg min^{-1} after deposition, with the arsenic cell valve open down to 350 °C.

Atomic force microscopy (AFM) and Kelvin force microscopy (KFM) images were taken with a PicoPlus 5500 (Agilent) system. The images consisted of 1024 × 1024 pixels and were taken in the dynamic mode, with silicon cantilevers having a nominal radius of 8 nm and a nominal force constant of 40 N/m (Bruker). The KFM measurements were carried out simultaneously to the topographic ones using Pt-coated cantilevers (AppNano-ANSCM-PT) with a nominal radius smaller than 40 nm. In this mode, the image records contact potential difference (CPD) whose changes are related to local changes in the surface potential. The resistance images were taken with a Nanobserver equipment and an external Resiscope module (both from Concept Scientific Instruments, France), operating in the soft Resiscope mode with diamond-coated cantilevers (Nanosensors-CDT-FMR) that had a radius of curvature in the 100–200-nm range and a force constant close to 6 N/m. The images were treated and analyzed using the free software Gwyddion [43].

The morphology of the InAs/Si samples was also examined with the aid of a high-resolution field-emission scanning electron microscope (FEI Nova NanoSEM 230), working at 50 V-30 kV and equipped with an EDX detector (EDAX Genesis XM2i) for quantitative analysis. Cross-sectional specimens suitable for high-resolution transmission electron microscopy (HRTEM) characterization were prepared using a focused ion beam (FIB) Helios 600 dual-beam system and examined in a Philips

Tecnai F20 TEM/STEM operating at 200 keV.

3. Results and discussion

3.1. InAs growth on nanostructured Si substrates

The InAs growth mode on the patterned Si substrate was investigated by using a combination of HRSEM and scanning probe microscopy techniques. The scanning electron micrographs gathered in Fig. 1(a) and 1(b) show the morphology variation of the Si nanotemplate after deposition of a nominal thickness of 100 ML and 125 ML InAs, respectively. As depicted in Fig. 1(a), the Si pattern consisted of a non-symmetric 480 nm–pitch grid along two orthogonal $\langle 1\,1\,0 \rangle$ directions with linewidths of 30 and 120 nm, respectively. After supply of the first 100 ML InAs, a widening of the pattern lines is clearly observable (Fig. 1 (b)), resulting from two-dimensional growth of InAs on the different facets of the patterned Si substrate. A closer examination of this sample with the AFM (Fig. 2) revealed the decoration of the $\langle 1\,1\,0 \rangle$ -oriented line edges of the template with InAs material, which we attribute to the migration of In adatoms from the (1 1 1)-wall facets to the top (0 0 1) surface edges, where its incorporation is kinetically more favorable. With further supply of InAs (125 ML) on the Si substrate, the strain accumulated on the (0 0 1) top facets bounded by $\langle 1\,1\,0 \rangle$ edges as well as on the (0 0 1) facets of the trenches triggers the 2D-to-3D growth mode transition. This results in the formation of linear arrays of QDs along both $\langle 1\,1\,0 \rangle$ directions and a random distribution of QDs at the trenches, as depicted in Fig. 1(c). Considering that it was necessary to supply an excess of 125 ML InAs to reach the 2 ML critical thickness for QD formation, the calculated In sticking coefficient on the Si surface at 490 °C is approximately 0.02.

After supply of 230 ML InAs, the nanodots on the (0 0 1) facets continue to grow in size. Meanwhile, the InAs material growing on one of the pattern walls, most likely in the (1 1 1)B orientation, reaches the critical thickness for the 2D-to-3D growth mode transition and the formation of new QDs via the S-K mechanism is observed. The AFM and KFM images gathered in Fig. 3 illustrate this change in morphology. A detail of the linear arrays of QDs formed along one of the $\langle 1\,1\,0 \rangle$ directions of the nanostructured Si substrate can be seen in Fig. 3(c). Previous scanning tunneling microscopy investigations relative to InAs growth on the Si(1 1 1) surface have demonstrated that initial surface reconstruction exerts a strong influence on growth mode and polarity. While InAs(1 1 1)A growth takes place in a two-dimensional manner on the In-terminated Si(1 1 1)-(4 × 1) surface, large InAs(1 1 1)B three-dimensional islands are formed on the As-terminated Si(1 1 1)-(7 × 7) and (1 × 1) surfaces [44]. Therefore, growth of QDs on the Si(1 1 1) facets under the As-rich conditions of our experiments is most likely to occur in the (1 1 1)B orientation. This preferential growth is favored by the predominant bonds formed between Si and As at the onset of growth, which has been established by core-level photoemission spectroscopy [45]. The absence of QDs in other areas of the nanopatterned substrate may be due to the existence of facets where 2D growth is preferred, e.g., (1 1 0) or (1 1 1) facets with alternate interfacial configurations resulting from the exchange reactions that involve interdiffusion of Si with the arriving In and As atoms. Such alternate configurations have been calculated to have a significantly lower total energy than the exclusive interfacial bonding of Si to As mentioned above and do not necessarily lead to the abovementioned (7 × 7) or (1 × 1) surface reconstructions associated with 3D island growth [46,47].

3.2. InAs growth on nanostructured GaAs-on-Si substrates

The HRSEM images depicted in Fig. 4 illustrate the growth morphology after deposition of 2 ML InAs on the GaAs-coated Si substrate under different experimental conditions. The micrograph in Fig. 4 (a) illustrates the surface morphology of a GaAs-capped InAs/GaAs/Si sample, hereafter referred to as sample A, where InAs was grown at 0.2
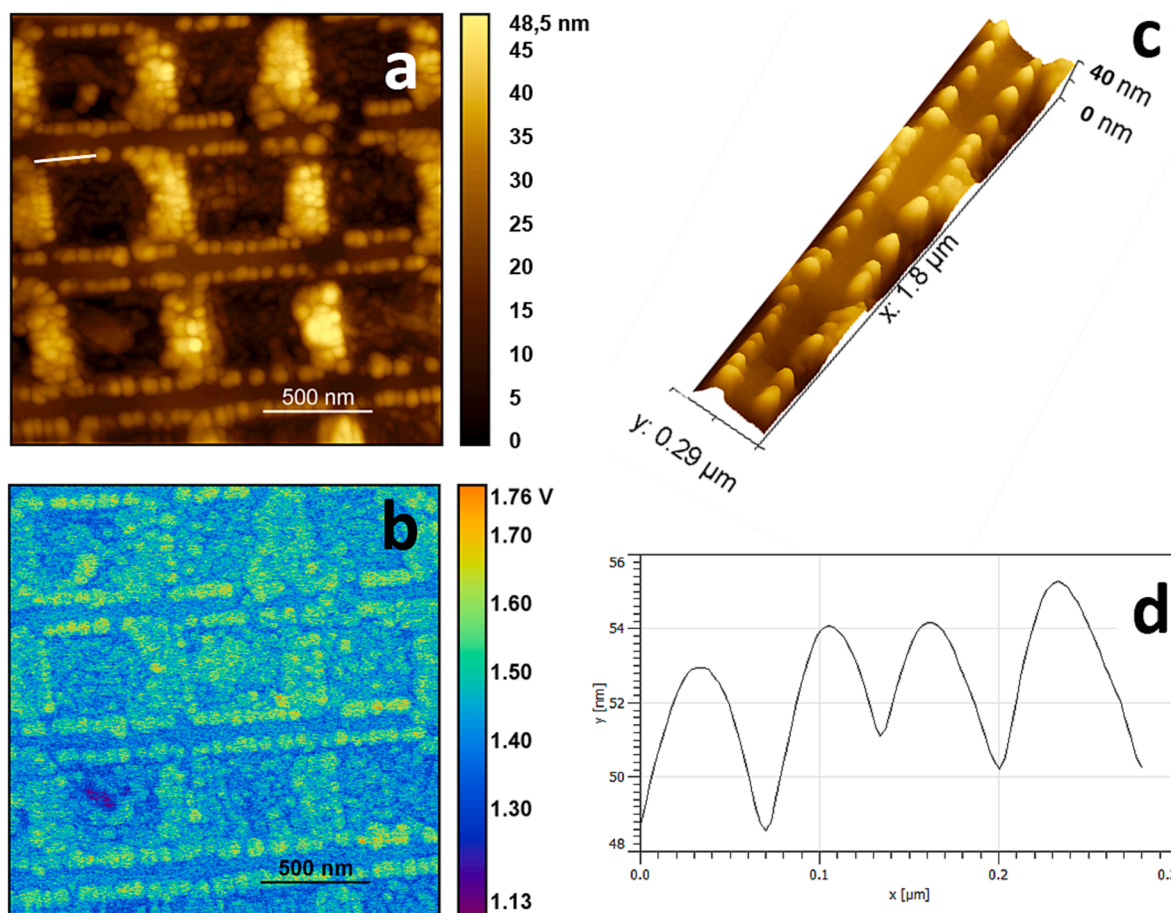
Fig. 3. (a) AFM topography and (b) KFM contact potential difference images of the surface after deposition of 230 ML InAs on the Si nanostructured substrate (image size: 2 μm × 2 μm). (c) Detail of the linear arrays of InAs QDs formed along one of the ⟨1 1 0⟩ -oriented mesa stripes and (d) cross-section profile of a dot chain along the ⟨1 1 0⟩ direction extracted from (a).

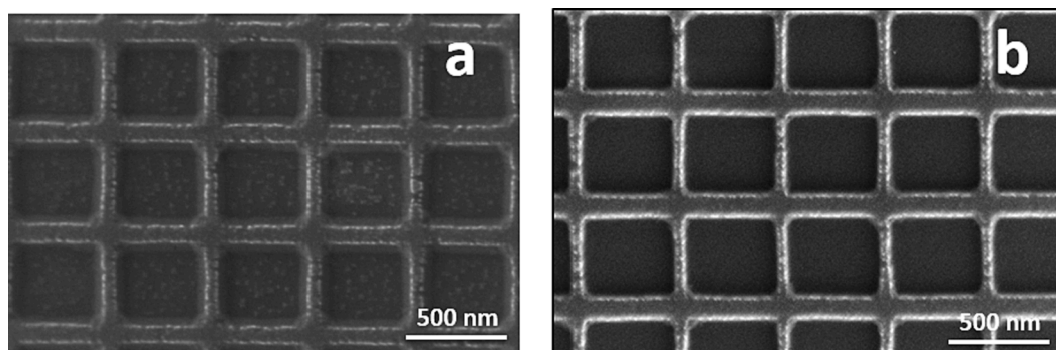**Fig. 4.** HRSEM images showing the surface morphology of GaAs/2 ML InAs samples grown on GaAs-on-Si substrates at 490 °C (a) at 0.2 ML s^{-1} with As/In flux ratio of 16 (Sample A) and (b) at 0.1 ML s^{-1} with As/In flux ratio of 32 (Sample B).

ML s^{-1} with an As/In flux ratio of 16. Fig. 4(b), in turn, shows the surface morphology of sample B, which has the same structure as sample A but was grown at 0.1 ML s^{-1} with an As/In flux ratio of 32. As observed in nanostructured Si substrates, QDs nucleate preferentially along the ⟨1 1 0⟩ -oriented edges of the GaAs-on-Si template in both samples as well as on the trenches in sample A. This indicates that the same kinetic- and strain-driven mechanisms operate on both substrates. But in contrast to Si substrates, the critical thickness for the S-K growth mode transition is the same as on a planar GaAs(0 0 1) substrate, i.e., ≈2 ML InAs, clearly due to the near-unity sticking coefficient of In on the GaAs surface at the temperature of our experiments [42]. In comparison with

sample A, the morphology of the dots nucleated along the ⟨1 1 0⟩ edges in sample B has not suffered any significant variation by lowering the growth rate. But it modifies the nucleation kinetics on the bottom (0 0 1) facets, preventing the formation of QDs on the trenches.

To further investigate this effect, the trench morphology of both samples was examined in detail using AFM. The results are shown in Fig. 5. QDs with a heigh of ∼ 3 nm, with a density of ∼ 4 × 10^{10} dots cm^{-2} are observed in sample A (Fig. 5(a)) while the trenches of sample B are fully covered with two-dimensional islands of monolayer and bilayer height (Fig. 5(b)), indicating that the wetting layer has not undergone the S-K transition yet in the sample grown at a lower rate. To account for
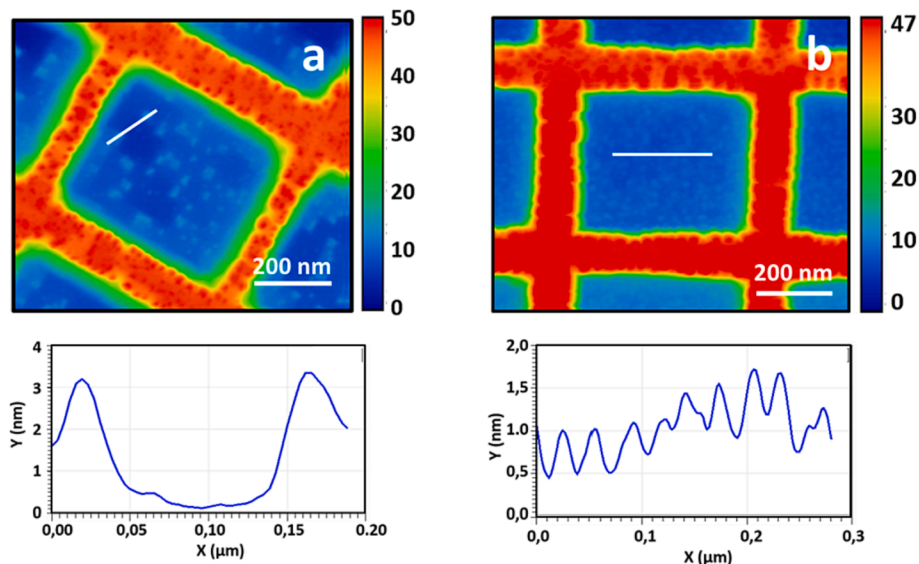
Fig. 5. AFM images showing the effect of the InAs deposition rate on the trench morphology of the GaAs-on-Si pattern: (a) sample A grown at 0.2 ML s^{-1} (image size: 870 nm × 750 nm) and (b) sample B grown at 0.1 ML s^{-1} (image size: 920 nm × 750 nm).

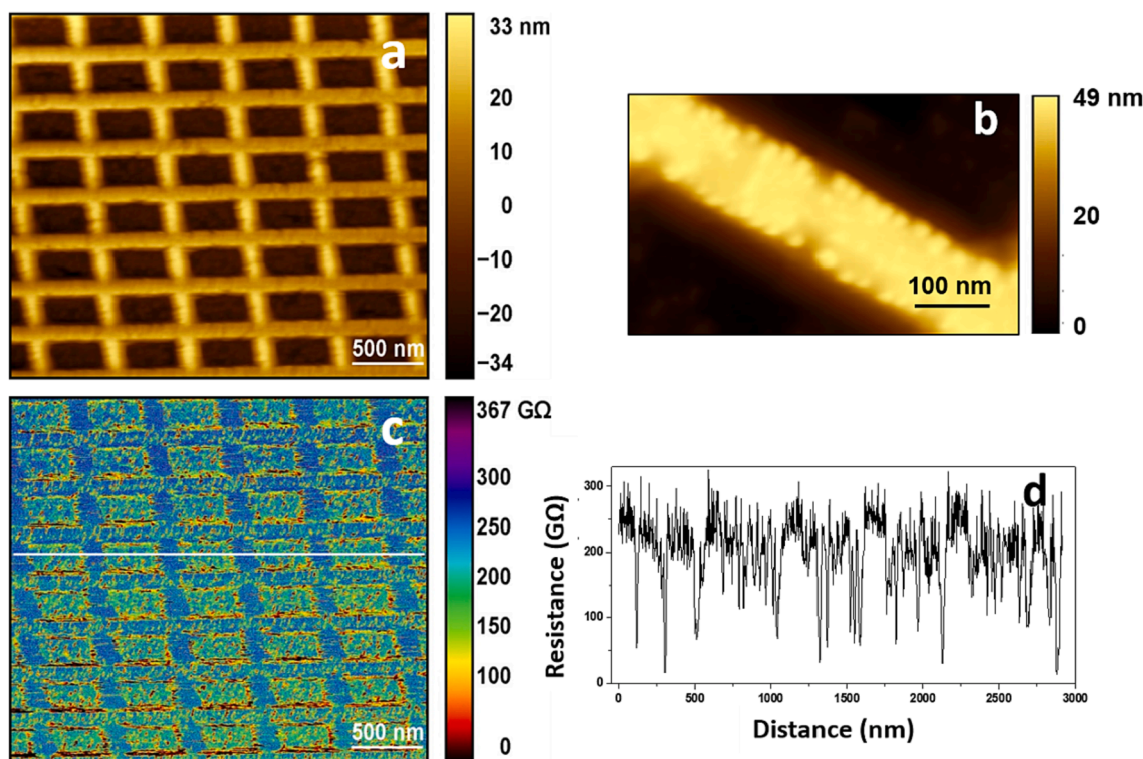**Fig. 6.** (a) AFM (3.0 μm × 2.5 μm) image of sample A (GaAs/2 ML InAs) grown on the GaAs-on-Si nanopattern with (b) a detail (400 nm × 220 nm) of the arrays of QDs formed on the ⟨110⟩ -oriented edges and (c) corresponding C-AFM image with (d) resistance profile taken across several trenches in the ⟨110⟩ direction.

these differences in growth kinetics, we must bear in mind that the lower flux of the group III element reaching the surface in sample B results in a longer diffusion length of the indium adatoms. This facilitates the preferential migration of In adatoms to those surface sites with lower energy, such as the ⟨110⟩ -oriented edges, where incorporation occurs rapidly, leading to the formation of QDs. However, the fraction of In adatoms available to react with the As precursor species at the trenches results in a high density of two-dimensional islands, although it is not high enough to reach coalescence and form a continuous layer during the course of the experiment. Consequentially, the experimental growth

conditions used in sample B do not allow reaching the InAs critical thickness (2 ML) for three-dimensional growth to take place on the trenches, thus opening the possibility of restricting the growth of linear arrays of QDs to the ⟨110⟩ template edges by simply controlling the deposition rate.

Fig. 6 gathers topographic- and conductive-AFM images of sample A. A detail image of the QD arrays nucleated along the ⟨110⟩ -oriented edges of the template can be seen in Fig. 6(b). The regions of higher conductivity, shown in dark brown in the C-AFM image (Fig. 6(c)), correspond to those sites where InGaAs QDs have formed preferentially,
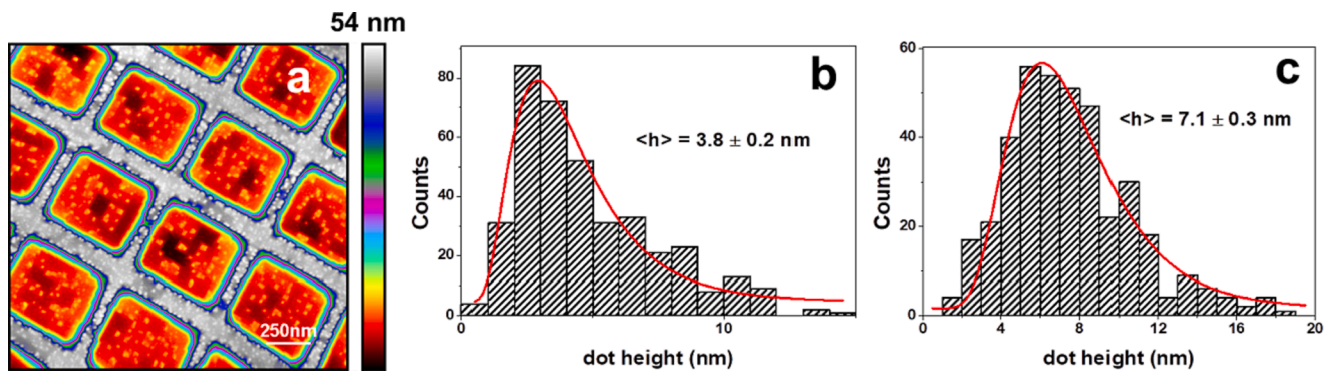
Fig. 7. (a) AFM image (2 μm × 2 μm) of sample A (GaAs/2 ML InAs) grown on the GaAs-on-Si nanopattern; histograms of the QD heights corresponding to (b) dots nucleated along the ⟨1 1 0⟩ -oriented edges and (c) dots nucleated on the trenches. The fitting to a log-normal function (red solid line) is shown for both histograms together with the average dot height < h > obtained from the fitting. (For interpretation of the references to colour in this figure legend, the reader is referred to the web version of this article.)
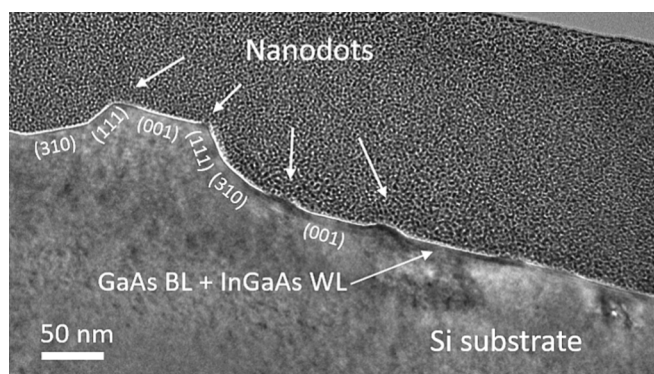

Fig. 8. Cross-section TEM image (71.000 ×) of sample A (GaAs/2 ML InAs) grown on the GaAs-on-Si nanopattern at 490 °C.

i.e., ⟨1 1 0⟩ edges and bottom of the trenches. Even though this sample is covered by a 5-nm-thick GaAs capping layer and comparisons should be made with caution, Fig. 6(b) evidences a reduction in dot size as well as an improvement in lateral order and size uniformity in the arrays grown on the GaAs-on-Si substrate in comparison to those grown directly on Si (Fig. 3(c)). In order to quantify this effect, the size distribution of QDs nucleated at different locations of the GaAs-on Si substrate was investigated. Height distributions (HD) rather than lateral size distributions were analyzed since the latter can be largely affected by tip convolution effects. The analysis was performed on the 2 μm × 2 μm AFM image shown in Fig. 7(a). Fig. 7(b) and 7(c) depict the HD of dots grown on the trenches and on the ⟨1 1 0⟩ -oriented edges, respectively. The histograms were fitted to a log-normal function [48]. Clearly, the distribution is quite narrow on the trench surface with a mean value of the dot height in the 3–4-nm range. In comparison, the distribution of dots nucleated on ⟨1 1 0⟩ -oriented edges is wider, rendering a mean value of the dot height of 7 nm. The variations in the wetting layer thickness and the absence of this layer in some areas (Fig. 7(a)), observed during examination of the sample, are the main factors behind the widening of the dot HDs. A separate analysis of the height distribution for dots nucleated along each of the two orthogonal ⟨1 1 0⟩ directions revealed that the average value of the dot height on the narrow stripes was close to 6 nm, whereas it reached 8 nm on the wider stripes. This anisotropy is conditioned by the structural inhomogeneities of the edges of the narrow lines (Fig. 1(a)), where the nucleation activation barrier is lower and, therefore, the deposition thickness at which 3D nucleation begins decreases. Due to this effect, the wetting layer thickness, as well as the size of the QDs, are reduced [49].

Fig. 8 depicts a TEM cross-section image of sample A. In addition to

the (0 0 1) facets where QDs were selectively nucleated, other facets with different crystallographic orientations, i.e., (1 1 1) and (3 1 0), were identified in the patterned substrate. The image revealed the formation of dots both along the ⟨1 1 0⟩ -oriented edges of the template and on the trench (0 0 1) facets of the GaAs-coated Si substrate, in good agreement with AFM measurements. An interfacial layer, originating from the ultrathin GaAs buffer layer and the $In_xGa_{1-x}As$ wetting layer formed prior to the S-K transition, can also be seen in the image. The structure and composition of this sample were then investigated by high-resolution TEM (HRTEM) analysis of the QDs formed at different substrate locations as well as the underlying wetting layer. All measurements were taken in the [0 1 1] zone axis of the Si substrate.

Fig. 9(a) depicts a high-resolution image of a nanodot grown on the edge of one of the ⟨1 1 0⟩ -oriented ridges of the virtual Si substrate. The GaAs buffer layer and the InGaAs wetting layer are not distinguishable in the image. The dot width and height determined from this image were 31 and 12 nm, respectively. The fast Fourier transform (FFT) of the complete image, which simulates the experimental electron diffraction pattern (EDP), can be seen in Fig. 9(b). The resulting EDP is consistent with an FCC structure with a uniform lattice constant since the diffraction spots are neither elongated nor double. This result confirms the absence of a buffer/wetting layer with composition and lattice constant different from those of the dot. The most plausible explanation for this result is that substrate erosion has occurred, favored by In-Ga intermixing that draws material from the buffer and wetting layers to form the InGaAs island at the step edge. Therefore, in addition to the incoming flux of the In and As$_2$ beams and the adatom migration from adjacent facets, the increase in dot volume occurring during the S-K transition also derives from the mass transfer that results from the stepedge erosion. Substrate erosion during InAs/GaAs(0 0 1) QD nucleation at step edges had been previously observed in AFM studies [50]. The TEM study presented here confirms these observations, revealing the absence of wetting and GaAs buffer layers underneath the dots as a result of the erosion process. To investigate further the growth of QDs on the ⟨1 1 0⟩ -oriented edges, we analyzed the FFT of the image region enclosed in the dashed square of Fig. 9(a), which is depicted in Fig. 9(c). In this case, we observed weak double spots next to the main reflections. The inverted image shown in Fig. 9(d) was extracted by selecting the (1 1 1) weak spots in the FTT shown in Fig. 9(c), which revealed a nonuniform spatial distribution of the dot chemical composition and lattice strain, attributable to the segregation of In toward the surface during the formation of the alloyed InGaAs island. Although the resolution of the HRTEM image did not allow us to determine the exact composition of the different regions of the QD, an average composition of $In_{0.52}Ga_{0.48}As$ was, nevertheless, calculated for the dot from the (1 1 1) reflections.

The results from high-resolution TEM analysis of a nanodot formed on the trench (0 0 1) facet in sample A are gathered in Fig. 10. Like dots
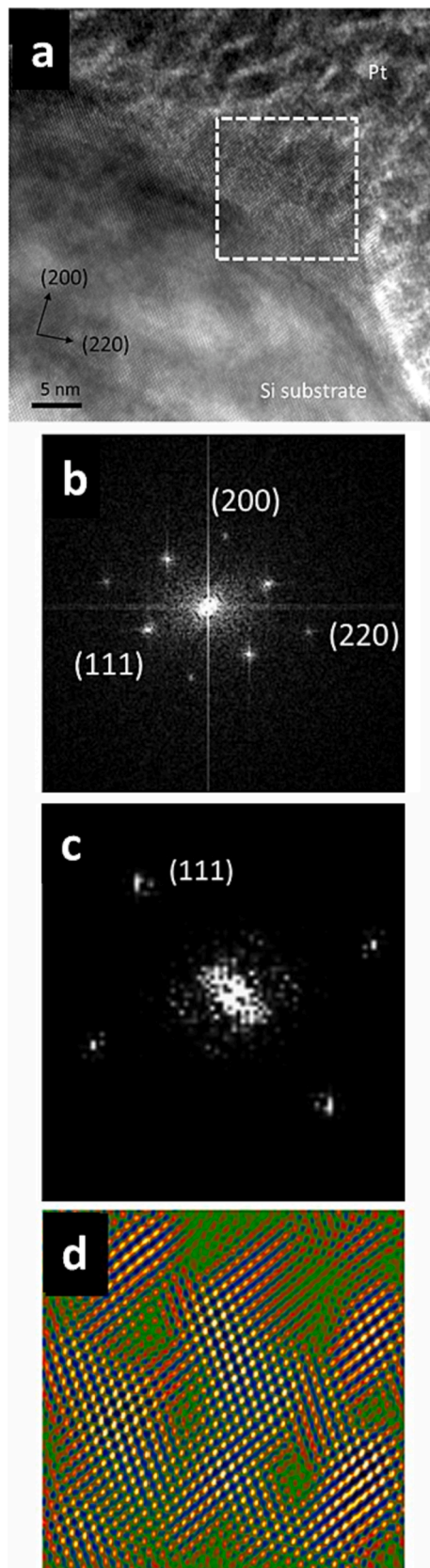
Fig. 9. (a) [0 1 1] HRTEM image of one of the nanodots formed along a ⟨1 1 0⟩ -oriented edge of the GaAs-on Si substrate, (b) FFT of the complete TEM image shown in (a), (c) FFT of the nanodot region enclosed in the dashed square shown in (a), and (d) inverted image extracted from the $(1\bar{1}1)$ and $(\bar{1}1\bar{1})$ elongated spots shown in (c).

formed on the template edges, those nucleated on the trenches are dislocation-free, i.e., coherent and larger in size. They are approximately 40 nm in diameter and 3–4 nm in height, and its cross-section suggests a truncated pyramid shape, as shown in Fig. 10(a). In consonance with this, the absence of dislocations in the interfacial layer reflects that both the buffer and the wetting layer had grown pseudomorphically strained on the nanostructured substrate. Fig. 10(b) depicts the FFT corresponding to the complete HRTEM image in (a), where elongated $(1\bar{1}1)$ and $(\bar{1}1\bar{1})$ diffraction spots are revealed, in contrast with the FFT of the dots nucleated on the ⟨1 1 0⟩ step edges shown in Fig. 9(b). Fig. 10(c) shows the inverted image obtained from the selection of the elongated diffraction around the $(1\bar{1}1)$ and $(\bar{1}1\bar{1})$ spots of the FFT in Fig. 10(b). As can be observed in the inverted image, this diffraction corresponds to the layer located between the dot and the Si substrate. Moreover, the elongated feature is indicative of the existence of a compositional gradient in this layer that results from In segregation and Ga-In intermixing between the GaAs buffer layer and the wetting layer during the S-K transition. The differences observed in the $(1\bar{1}1)$ and $(\bar{1}1\bar{1})$ diffraction spots are a reflection of the different formation mechanisms that originate both types of QDs. While the dots nucleated on (0 0 1) trenches of the GaAs-on-Si substrate basically follow the same S-K mechanism as on a planar GaAs (0 0 1) substrate, the S-K transition at the ⟨1 1 0⟩ -oriented edges occurs more readily, not only because nucleation is energetically more favorable at step edges but also mainly due to the extra mass flow received by the dots coming both from adjacent facets and from the erosion of the wetting and buffer layers at the step edge. As a result of this change in growth kinetics, the dots along the ⟨1 1 0⟩ direction have a larger volume, do not exhibit an underlying buffer or wetting layer, and despite the local variations in In composition observed, they are defect-free and coherently strained.

4. Conclusion

The nucleation of InAs on nanostructured bare- and GaAs-coated Si (0 0 1) substrates by MBE has been investigated with the aim of creating one- and two-dimensional arrays of InAs and InGaAs QDs for quantum information applications. We have shown that growth of InAs on both types of substrate leads to preferential nucleation along the ⟨1 1 0⟩ -oriented edges of the nanostructured template, forming periodic arrays of QDs in both directions. Our results have demonstrated that the deposition of an ultra-thin GaAs buffer layer on the nanostructured Si substrate allows growing arrays of dislocation-free InGaAs QDs along orthogonal ⟨1 1 0⟩ directions with a significant better crystal quality and size uniformity than those directly grown on Si and at a lower cost than those grown on a GaAs substrate. In contrast to QDs nucleated on the planar (0 0 1) trenches of the GaAs-coated Si substrate, dots formed along the ⟨1 1 0⟩ step edges have a larger volume. This is mainly due to kinetically-driven In adatom incorporation from adjacent (1 1 1) facets and substrate erosion at the step edge, which causes mass transfer from the underlying wetting and buffer layers into the growing island. Finally, we have demonstrated that the existing differences in growth kinetics at different locations of the nanostructured substrate can be advantageously exploited to limit the nucleation of linear arrays of QD along ⟨1 1 0⟩ step edges by simply modifying the InAs deposition rate. Nevertheless, other approaches that are under investigation in our laboratory to attain this aim include the nanofabrication of alternative templates with trenches where no (0 0 1) nanofacets are present.

Declaration of Competing Interest

The authors declare that they have no known competing financial interests or personal relationships that could have appeared to influence the work reported in this paper.
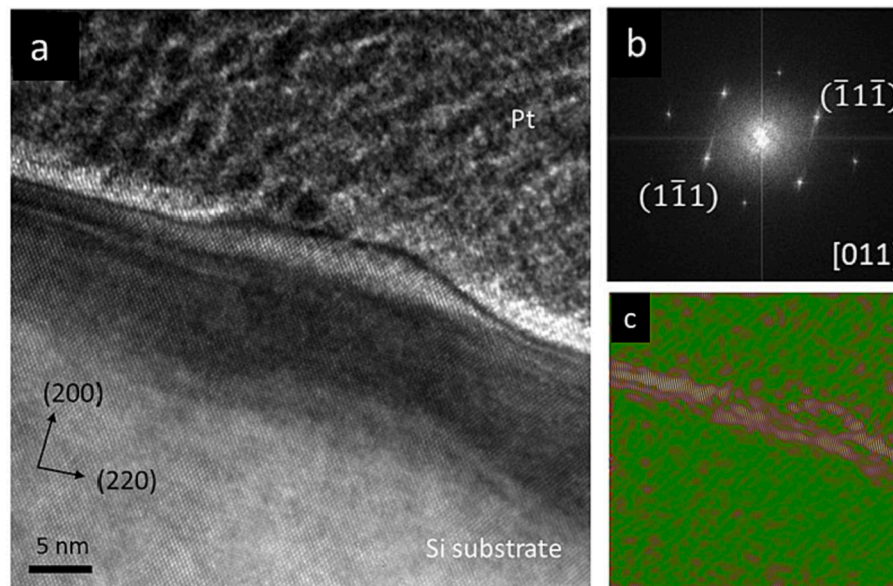
Fig. 10. (a) [0 1 1] HRTEM image of a nanodot formed on the (0 0 1) facet of a trench in the GaAs-on Si substrate virtual template, (b) FFT of the complete TEM image shown in (a), and (c) inverted image extracted from the ($1\bar{1}$ 1) and ($\bar{1}1\bar{1}$) elongated spots shown in (b).

Data availability

Data will be made available on request.

Acknowledgments

References

[1] D. Bimberg, M. Grundmann, N.N. Ledentsov, Quantum Dot Heterostructures, John Wiley & Sons, Chichester, New York, 1999.

[2] J.C. Norman, R.P. Mirin, J.E. Bowers, Quantum dot lasers-History and future prospects, J. Vac. Sci. Technol. A 39 (2021), 020802, https://doi.org/10.1116/6.0000768.

[3] T. Kageyama, K. Nishi, M. Yamaguchi, R. Mochida, Y. Maeda, K. Takemasa, Y. Tanaka, T. Yamamoto, M. Sugawara, Y. Arakawa, Extremely high temperature (220°C) continuous-wave operationof 1300-nm-range quantum dot-lasers. The European Conference on Lasers and Electro-Optics, Optical Society of America, 2011.

[4] A. Abdollahinia, S. Banyoudeh, A. Rippien, F. Schnabel, O. Eyal, I. Cestier, I. Kalifa, E. Mentovich, G. Eisenstein, and J.P. Reithmaier, Temperature stability of static and dynamic properties of 1.55 μm quantum dot lasers, Opt. Express 26 (2018) 6056-6066. https://doi.org/ 10.1364/OE.26.006056.

[5] H. Schmeckebier, C. Meuer, D. Bimberg, C. Schmidt-Langhorst, A. Galperin, C. Schubert, Quantum dot semiconductor optical amplifiers at 1.3 μm for applications in all-optical communication networks, Semicond. Sci. Technol. 26 (2010), 014009, https://doi.org/10.1088/0268-1242/26/1/014009.

[6] T. Umezawa, K. Akahane, A. Kanno, T. Kawanishi, Investigation of a 1.5-μm-wavelength InAs-quantum-dot absorption layer for high-speed photodetector, Appl. Phys. Express 7 (2014), 032201, https://doi.org/10.7567/APEX.7.032201.

[7] Y. Arakawa, M.J. Holmes, Progress in quantum-dot single photon sources for quantum information technologies: A broad spectrum overview, Appl. Phys. Rev 7 (2020), 021309, https://doi.org/10.1063/5.0010193.

[8] A. Chatterjee, P. Stevenson, S. De Franceschi, A. Morello, N.P. de Leon, F. Kuemmeth, Semiconductor qubits in practice, Nat. Rev. Phys. 3 (2021) 157–177, https://doi.org/10.1038/s42254-021-00283-9.

[9] B.A. Joyce, D.D. Vvedensky, Quantum dots in the InAs/GaAs system, in: B.A. Joyce, P.C. Kelires, A.G. Naumovets, D.D. Vvedensky, D.D. (Eds.), Quantum Dots: Fundamentals, Applications, and Frontiers, NATO Science Series, vol 190. Springer, 2005, pp. 1-26. https://doi.org/10.1007/1-4020-3315-X_1.

[10] B.A. Joyce, D.D. Vvedensky, Self-organized growth on GaAs surfaces, Mater. Sci. Eng. R 46 (2004) 127–176, https://doi.org/10.1016/j.mser.2004.10.001.

[11] P. Tejedor, L. Díez-Merino, I. Beinik, C. Teichert, Conductive atomic force microscopy study of InAs growth kinetics on vicinal GaAs(110), Appl. Phys. Lett. 95 (2009), 123103, https://doi.org/10.1063/1.3232234.

[12] L. Díaz-Merino, P. Tejedor, InGaAs/GaAs(110) quantum dot formation via step meandering, J. Appl. Phys. 110 (2011), 013106, https://doi.org/10.1063/1.3608047.

[13] K.E. Sautter, K.D. Vallejo, P.J. Simmonds, 2020. Strain-driven quantum dot self-assembly by molecular beam epitaxy. J. Appl. Phys. 128, 031101. https://doi. org/10.1063/5.0012066.

[14] S. Irvine, P. Capper, Metalorganic Vapor Phase Epitaxy (MOVPE): Growth, Materials Properties, and Applications, John Wiley & Sons, New York, 2019.

[15] D. Leonard, M. Krishnamurthy, C.M. Reaves, S.P. Denbaars, P.M. Petroff, Direct formation of quantum-sized dots from uniform coherent islands of InGaAs on GaAs surfaces, Appl. Phys. Lett. 63 (1993) 3203, https://doi.org/10.1063/1.110199.

[16] M. Biehl, F. Much, Simulation of wetting-layer and island formation in heteroepitaxial growth, Europhys. Lett. 63 (2003) 14–20, https://doi.org/10.1209/epl/i2003-00471-9.

[17] A. Ohtake, M. Ozeki, J. Nakamura, Strain Relaxation in InAs/GaAs(111)A Heteroepitaxy, Phys. Rev. Lett. 84 (2000) 4665, https://doi.org/10.1103/PhysRevLett.84.4665.

[18] J.G. Belk, D.W. Pashley, C.F. McConville, B.A. Joyce, T.S. Jones, Surface morphology during strain relaxation in the growth of InAs on GaAs(110), Surf. Sci. 410 (1998) 82–98, https://doi.org/10.1016/S0039-6028(98)00300-8.

[19] G.E. Cirlin, N.K. Polyakov, V.N. Petrov, V.A. Egorov, D.V. Denisov, B.V. Volovik, V. M. Ustinov, Z.I. Alferov, N.N. Ledenstov, R. Heitz, D. Bimberg, N.D. Zakharov, P. Werner, U. Gösele, Heteroepitaxial growth of InAs on Si: The new type of quantum dots, Mater. Phys. Mech. 1 (2000) 15–19.

[20] L. Hansen, A. Ankudinov, F. Bensing, J. Wagner, G. Ade, P. Hinze, V. WagnerJ, A. W. Geurts, Growth and characterization of InAs quantum dots on Silicon, Phys. Status Solidi 224 (2001) 515–519, https://doi.org/10.1002/1521-3951(200103)224:2.

[21] T. Alzoubi, M. Usman, M. Benyoucef, J.P. Reithmaier, Growth of InAs quantum dots and dashes on silicon substrates: Formation and characterization, J. Cryst. Growth 323 (2011) 422-425. https://doi. org/10.1016/jcrysgro.2010.11.170.

[22] H. Lan, Y. Ding, Ordering, positioning and uniformity of quantum dot arrays, Nano Today 7 (2012) 94–123, https://doi.org/10.1016/j.nanotod.2012.02.006.

[23] L.N. McCabe, J.M.O. Zide, Techniques for epitaxial site-selective growth of quantum dots, J. Vac. Sci. Technol, A 39 (2021), 010802, https://doi.org/10.1116/6.0000623.

[24] J. Große, M. von Helversen, A. Koulas-Simos, M. Hermann, S. Reitzenstein, Development of site-controlled quantum dot arrays acting as scalable sources of indistinguishable photons, APL Photon. 5 (2020) 096107, https://doi.org/10.1063/5.0013718.

[25] A.A. Tang, Nanofabrication Fundamentals and Applications, World Scientific, Singapore, 2008.

[26] H. Nakamura, S. Kohmoto, T. Ishikawa, K. Asakawa, Novel nano-scale site-controlled InAs quantum dot assisted by scanning tunneling microscope probe,

Physica E: Low-dimensional Syst. Nanostruct. 7 (2000) 331–336, https://doi.org/10.1016/S1386-9477(99)00335-5.

[27] S. Ohkouchi, Y. Nakamura, H. Nakamura, K. Asakawa, Indium nano-dot arrays formed by field-induced deposition with a Nano-Jet Probe for site-controlled InAs/GaAs quantum dots, Thin Solid Films 464 (2004) 233–236, https://doi.org/10.1016/j.tsf.2004.06.047.

[28] Y. Wang, S. Chen, Y. Yu, L. Zhou, L. Liu, C. Yang, M. Liao, M. Tang, Z. Liu, J. Wu, W. Li, I. Ross, A.J. Seeds, H. Liu, S. Yu, Monolithic quantum-dot distributed feedback laser array on silicon, Optica 5 (2018) 528–533, https://doi.org/10.1364/OPTICA.5.000528.

[29] C. Shang, Y. Wan, J.C. Norman, N. Collins, I. MacFarlane, M. Dumont, S. Liu, Q. Li, K.M. Lau, A.C. Gossard, J.E. Bowers, Low-threshold epitaxially grown 1.3 μm InAs quantum dot lasers on patterned (001) Si, IEEE J. Sel. Topics Quantum Electron. 25 (2019) 1502207, https://doi.org/10.1109/JSTQE.2019.2927581.

[30] Y. Xue, W. Luo, S. Zhu, L. Lin, B. Shi, K.M. Lau, 1.55μm electrically pumped continuous wave lasing of quantum dash lasers grown on silicon, Opt. Express 28 (2020) 18172-18179. https://doi.org/101364/OE.392120.

[31] J.C. Norman, D. Jung, Y. Wan, J.E. Bowers, Perspective: The future of quantum dot photonic integrated circuits, APL Photonics 3 (2018), 030901, https://doi.org/10.1063/1.5021345.

[32] N. Kobayashi, K. Sato, M. Namikawa, K. Yamamoto, S. Watanabe, T. Kita, H. Yamada, H. Yamazaki, Silicon photonic hybrid ring-filter external cavity wavelength tunable lasers, J. Lightware Technol. 33 (2015) 1241–1246. https://opg.optica.org/jlt/abstract.cfm?URI=jlt-33-6-1241.

[33] Y.P. Kandel, H. Qiao, S. Fallahi, G.C. Gardner, M.J. Manfra, J.M. Nichol, Adiabatic quantum state transfer in a semiconductor quantum-dot spin chain, Nat. Commun. 12 (2021) 2156, https://doi.org/10.1038/s41467-021-22416-5.

[34] A.J. Sigillito, M.J. Gullans, L.F. Edge, M. Borselli, J.R. Petta, Coherent transfer of quantum information in a silicon double quantum dot using resonant swap gates, Npj Quantum Inf. 5 (2019) 110, https://doi.org/10.1038/s41534-019-0225-0.

[35] T. Nakajima, M.R. Delbecq, T. Otsuka, S. Amaha, et al., Coherent transfer of electron spin correlations assisted by dephasing noise, Nat. Commun. 9 (2018) 2133, https://doi.org/10.1038/s41467-018-04544-7.

[36] T.A. Baart, T. Fujita, C. Reichl, W. Wegscheider, L.M.K. Vandersypen, Coherent spin-exchange via a quantum mediator, Nat. Nanotechnol. 12 (2017) 26–30, https://doi.org/10.1038/nnano.2016.188.

[37] A.R. Mills, D.M. Zajac, M.J. Gullans, F.J. Schupp, T.M. Hazard, J.R. Petta, Shuttling a single charge across a one-dimensional array of silicon quantum dots, Nat. Commun. 10 (2019) 1063, https://doi.org/10.1038/s41467-019-08970-z.

[38] H. Flentje, P.-A. Mortemousque, R. Thalineau, A. Ludwig, A.D. Wieck, C. Bäuerle, T. Meunier, Coherent long-distance displacement of individual electron spins, Nat. Commun. 8 (2017) 501, https://doi.org/10.1038/s41467-017-00534-3.

[39] Y.B. Bolkhovityanov, O.P. Pchelyakov, GaAs epitaxy on Si substrates: Modern status of research and engineering, 51 (2008) 437-496. https://doi.org/10.1070/PU2008v051n05ABEH006529.

[40] R.J. Fischer, PhD Dissertation, University of Illinois at Urbana Champaign, 1986.

[41] C.h. Heyn, Stability of InAs quantum dots, Phys. Rev. B 66 (2002), 075307, https://doi.org/10.1103/PhysRevB.66.075307.

[42] H. Öfner, S.L. Surnev, Y. Shapira, F.P. Netzer, In overlayers on Si(111)7X7: Growth and evolution of the electronic structure, Phys Rev B 48 (1993) 10940–10949, https://doi.org/10.1103/PhysRevB.48.10940.

[43] D. Nečas, P. Klapetek, Gwyddion: an open-source software for SPM data analysis, Centr. Eur. J. Phys. 10 (2012) 181–188, https://doi.org/10.2478/s11534-011-0096-2.

[44] A. Ohtake, K. Mitsuishi, Polarity controlled InAs{111} films grown on Si(111), J. Vac. Sci. Technol. B 29 (2011), 031804, https://doi.org/10.1116/1.3589807.

[45] R.D. Bringans, M.A. Olmstead, R.I.G. Uhrberg, R.Z. Bachrach, Interface formation of GaAs with Si(100), Si(111), and Ge(111): Core-level spectroscopy for monolayer coverages of GaAs, Ga, and As, Phys. Rev. B 36 (1987) 9569, https://doi.org/10.1103/PhysRevB.36.9569.

[46] J.E. Northrup, Atomic structure of one monolayer of GaAs on Si(111), Phys. Rev. B 37 (1988) 8513, https://doi.org/10.1103/PhysRevB.37.8513.

[47] J.R. Patel, P.E. Freeland, M.S. Hybertsen, D.C. Jacobson, J.A. Golovchenko, Location of atoms in the first monolayer of GaAs on Si, Phys. Rev. Lett. 59 (1987) 2180, https://doi.org/10.1103/PhysRevLett.59.2180.

[48] R.B. Bergmann, A. Bill, On the origin of logarithmic-normal distributions: An analytical derivation, and its application to nucleation and growth processes, J. Cryst. Growth 310 (2008) 3135–3138, https://doi.org/10.1016/j.jcrysgro.2008.03.034.

[49] N.E. Chernenko, S.V. Balakirev, M.M. Eremenko, M.S. Solodovnik, Effect of morphology features of patterned surface on the nucleation processes of In/GaAs nanostructures during droplet epitaxy, J. Phys.: Conf. Series 1410 (2019), 012007, https://doi.org/10.1088/1410/1/012007.

[50] E. Placidi, F. Arciprete, V. Sessi, M. Fanfoni, F. Patella, A. Balzarotti, Step erosion during nucleation of InAs/GaAs (001) quantum dots, Appl. Phys. Lett. 86 (2005), 241913, https://doi.org/10.1063/1.1946181.